Wavelet-based Optimization of Surface Reconstruction

Péter Kocsis, Petra Balla and Ákos Antal

Department of Mechatronics, Optics and Mechanical Engineering Informatics,
Budapest University of Technology and Economics
Műegyetem rkp. 3, 1111 Budapest, Hungary

E-mail: petra.balla@mogi.bme.hu, antal.akos@mogi.bme.hu

Abstract: By the development of artificial Intelligence – whether unintentionally – we are constantly trying to mimic the human senses. Biomimicry, as the starting point, is an engineering approach to emulate nature's well working patterns and strategies. Our goal is to create a standalone artificial system which can respond adequately to various environmental impacts without human intervention. In order to detect these influences over the accuracy of human limitations, the most advanced sensors are needed both in software and hardware. The development in computing power highlights some forgotten algorithms, which were neglected because their complexity made them inefficient on early computers. One of these methods is the Wavelet-Transform Profilometry (WTP) of which successful application is demonstrated in this paper. WTP is a three-dimensional profilometric surface reconstruction algorithm in which orthogonal trajectories are used for high-level signal processing of huge datasets. Our goal was to find a high-precision solution for surface reconstruction by replacing the processing software with advanced mathematical methods rather than use more expensive optical systems.

Keywords: profilometry; Wavelet; reconstruction; machine vision

1 Introduction

Accurate surface reconstruction plays an important role in the field of non-destructive measurement technology that is why the concept of human eye can be only a starting point. There are two main parts of these systems, which can be improved: the optics and the processing algorithm. With the development of computing power the price gap between them became wider and wider. Therefore, we should focus on complex mathematical methods to reach higher-level precision, like Hilbert-, S-, Gábor-, Fourier- or Wavelet-transform. The industrial usage of three-dimensional scanners requires less noise sensitive methods because the machines are continuously vibrating in most places. The advantage of the

complex orthogonal methods is that the entire spatial analysis needs only one image and by increasing the number of the pixels of the image the function of frequency and the accuracy itself will be significantly improved. The first successful use of the one-dimensional Fourier-transformation was published in 1982 by M. Takeda [1], [2] and in 1982 Bone applied the two-dimensional algorithm successfully as well [3]. The method evolved since then and its use of scale became wider, making it possible to be able to reconstruct three-dimensional surfaces with it. In this paper, you can read a short presentation of the field of structured light techniques and profilometry, then Fourier- and Wavelet-transformations are presented as a sequel to our former research [4]. After, the main part Wavelet-transformation profilometry, the laboratory tests, the functional tests and the results will be presented. Finally, the conclusions and the development opportunities will follow.

2 Imaging Methods with Structures Lights

In machine vision the datasets are containing a two-dimensional matrix as an image. To obtain the depth value we can use density distribution (MRI, CT) or traditional surface analysis, in which the information is stored in given scaled scale values, or colour values by using vectors calculated with RGB (red-green-blue). The most common method is to project structured light on the surface with a projector, modulated illuminant by spatial light or laser matrix and capture the reflection with a detector. Each pixel of the digitally processed image has a matrix element and $\{I_{ij} = (i,j), i = 1,2,\dots,I; j = 1,2,\dots,J\}$ is characterizing the intensity, where (i, j) is the (x, y) coordinate of the projected pattern. The distorted image contains deformed patterns, which from; we can extract the depth information. Two main groups of methods can be distinguished by their dynamics, depending on the number of images the algorithm needs. The first one is a sequential, so called multi-shot method, in which we capture multiple images and the additional information can be calculated from the differences between them. We can use binary- and Graycode, phase shift method or a hybrid one. The more images means higher amount of data. Therefore, the method is very precise, but can be only used on static objects. Thanks to the colour information or the specific encoding schemes we can use single-shot methods to reconstruct surfaces from only one image. For this we can use constantly changing patterns like the 3D rainbow camera, band indexing procedures like colour codes, grayscale patterns, De Brujin series or special 2D grid indexing with pseudo-random binary array and colour-coded grids [5].

Figure1
De Brujin series

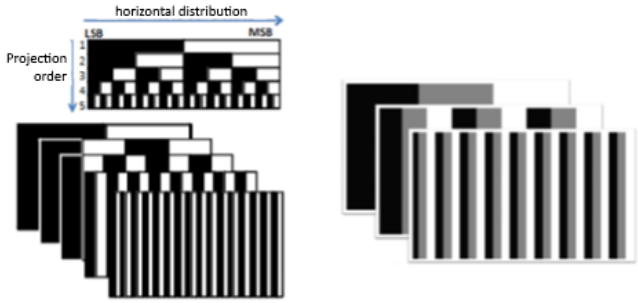

Figure 2
Binary and Gray coding [5]

3 Profilometry

Profilometry is one of the most researched fields of the last decade, although it has relatively short existence and it is also called Fringe Projection Technique. The name came from the fact that the base of this method is to create a specific projection pattern, which is projected and deforms on the surface. The layout is similar to the deflectometric and the triangulation methods, the main units are:

1.) Test object

2.) Projector

3.) Image capture unit (Camera)

4.) Image processing unit (Computer)

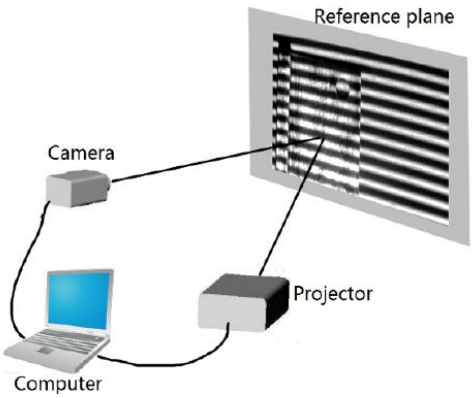

Figure 3
Fringe Projection Technique layout [6]

The method comprises the following steps: First, we select a periodically structured signal, project it on the object and record the distorted image from the surface. This signal is usually a sinusoidal pattern with known phase, the recording device is a camera, but in special cases we can use a system with image capture card. We read the image and process it with a chosen algorithm, then calculate the phase modulation and unwrap the phase. To manage this, we used MATLAB to store the scanned image in a three-dimensional colour matrix, which was reduced to two-dimensional with black and white transformation. The algorithm is mostly a Fourier-transformation or its modification, like the interpolating- or regressive Fourier-transformation, dilated Gabor-transformation, discrete cosine-transformation, S-transformation and Hilbert-transformation, or what we used is one- and two-dimensional Wavelet transformation. Finally, we are mapping the unwrapped values and perform phase- and depth conversion. The unwrapping is performed with a built-in unwrapping algorithm that we present in Sec. 6.

4 Fourier-Transform Analysis

Image processing is just one of the many options that Fourier-transform algorithm is capable of [7]. The three-dimensional surface reconstruction needs to capture of the deformed surface$(g(x,y))$, and a reference sample$(g_0(x,y))$ in the following ways:

$$g(x,y) = r(x,y)\sum_{n=-\infty}^{\infty} A_n e^{j(2\pi f_0 x + n\varphi(x,y))} \tag{1a}$$

$$g_0(x,y) = r_0(x,y)\sum_{n=-\infty}^{\infty} A_n e^{j(2\pi f_0 x + n\varphi(x,y))} \tag{1b}$$

where $r(x,y)$ and $r_0(x,y)$ are the concurrent components of the non-uniform reflections, A_n is the weighting factor, f_0 is the carrier frequency, $\varphi(x,y)$ and $\varphi_0(x,y)$ are the value of the phase. The spectrum is the Fourier-transform of the sum, which from we can filter and define the required components. The difference between the modulated signal and the reference signal can be calculated with inverse Fourier-transform:

$$\bar{g}(x,y) = A_1 r(x,y) e^{j(2\pi f_0 x + \varphi(x,y))} \tag{2a}$$

$$\bar{g}_0(x,y) = A_1 r_0(x,y) e^{j(2\pi f_0 x + \varphi(x,y))} \tag{2b}$$

The disadvantage of the procedure is that only frequency domain analysis is performable with it because it approximates the signal with sinusoidal harmonics. Therefore, the analysis does not have temporal localization properties and the time function cannot determine the examined frequency components. Due to the breakdown of the signal into plane waves, if the signal changes in one coordinate its Fourier-transform will change as well, that is why we cannot define the place of change. On the other hand, the overlapping can occur signal analysis errors because the sinusoidal signals cannot be ended in the block borders. We can eliminate these errors by using Wavelet-transform analysis [8].

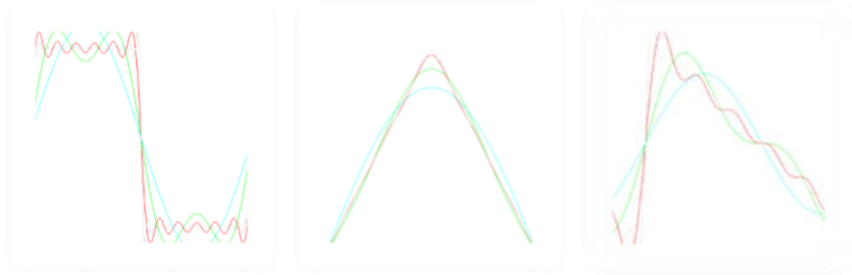

Figure 4
a) square wave approximation, b) Saw wave approximation, c) Triangle wave approximation

5 Wavelet-Transform Analysis

This spectral resolution method has been known since the beginning of the 20th Century, but became internationally known from the late 1980s thanks to Y. Meyer's and Stephane Mallatt's work [7], [9]. The advantage of this algorithm is that WTA divides the signals into so-called mother wavelets instead of sinusoidal, which have limited length and zero mean value. These properties eliminate the errors of FTA because the sharp changes in the frequency spectrum and their coordinates can be determined at the same time. So, time analysis – in our case spatial analysis – is also feasible with it.

Correspondingly to the Fourier-transform the additional information can be obtained from the difference between the signal under test (u) and the test function (v) using internal multiplying mathematical tools:

$$< u, v \geq |u||v| \cos(\theta) \tag{3}$$

If u and v is a unit, then the cosine of the angle between them determines the result, so it is limited into the $[-1, 1]$ interval. The harmonics of the sine function are regular and smooth while in case of Wavelet-transform analysis they are irregular and asymmetric, that is why the sharp and sudden changes can be detected easier. [10]

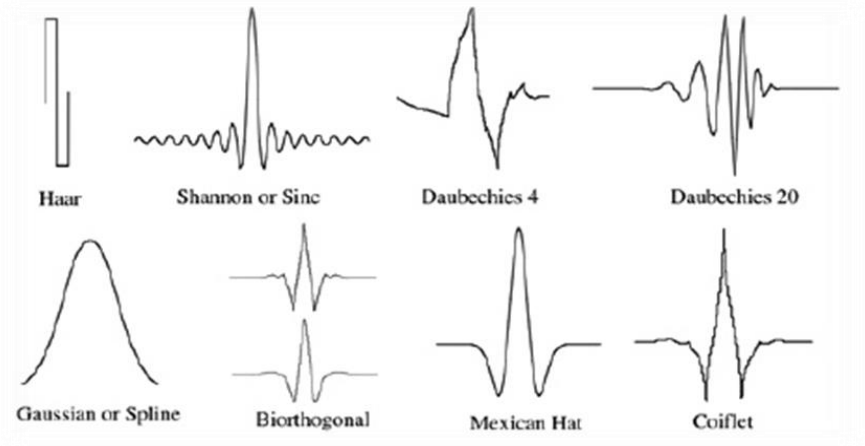

Figure 5
Wavelet signals

5.1 Mother Wavelets

Scale is one of the main properties of the wavelet groups; it declares the compression and stretching of the function. To obtain the depth value we need to use complex mother wavelets when the wavelet transform is a complex function of the scale and position. We can create countless mother wavelet types, but all of them need to fulfill the following correlation:

$$\int_{-\infty}^{\infty} \psi(t)dt = 0 \tag{4}$$

where$\psi(t)$ is the wavelet function and if $\omega = 0$ then $\psi(\omega) = 0$, which is the Fourier transform of the wavelet function. For the study we used the MATLAB provided complex mother wavelets:

- Complex Gaussian:

$$\psi_{Gaussian}(x) = \frac{d(C_p \exp(-ix) \exp(-x^2))^p}{dx^p} \tag{5}$$

- Complex Shannon:

$$\psi_{Shannon}(x) = \sqrt{f_b} \exp(2\pi i f_c x) \, (sinc(f_b x)) \tag{6}$$

- Complex Frequency B-spline:

$$\psi_{b-spline}(x) = \sqrt{f_b} \exp(2\pi i f_c x) \left[sinc\left(\frac{f_b x}{m}\right)\right]^m \tag{7}$$

- Complex Morlet:

$$\psi_{Morlet}(x) = \frac{1}{(f_b^2 \pi)^{\frac{1}{4}}} \exp(2\pi i f_c x) \exp(\frac{-x^2}{2f_b^2}) \tag{8}$$

5.2 Continuous Wavelet Transformation

The compression value (a) and the offset value (τ)of the base function defines a binary function

$$\mathrm{F(a,\tau)} = \frac{1}{\sqrt{a}} \int f(t) \psi\left(\frac{t-\tau}{a}\right) dt \tag{9}$$

where $\psi(t)$ is the basic wavelet function, $\psi\left(\frac{t-\tau}{a}\right)$ is the base function of the transformation, $\mathrm{F(a,\tau)}$ is the wavelet transformation itself. The two variables and the wavelet function declare the coefficients of the continuous wavelet transformation, but we need to concrete the parameters. Therefore, we can use a discrete equation as

$$F[m,n] = \frac{1}{\sqrt{a_0^{-m}}} \int f(t) \psi(a_0^m t - n\tau_0) dt \tag{10}$$

where a_0 is the base power of the compression and τ_0 determine the offsets value. It can be seen that the offset and the compression have to be given powers of the invariants to reach optional values. We can manage this by reducing the offset by half, if the compression is reduced by half as well, in this case we will not miss any part of the function and there will be no overlapping over and above the counting.

The transformation gives good time-resolution and bad frequency-resolution by high-frequency base functions and the opposite by low-frequency base function. The connection between the scale and frequency is clear: the higher scale parameter results higher strain of the mother-wavelet, so the correlation will be over a bigger part of the signal and the accuracy will drop. This means that we can use small values to perceive fast changes and slow ones for slow changes. The continuity comes from the fact that it is interpretable in every scale and the mother wavelets offset is continuous in the whole range of interpretation.

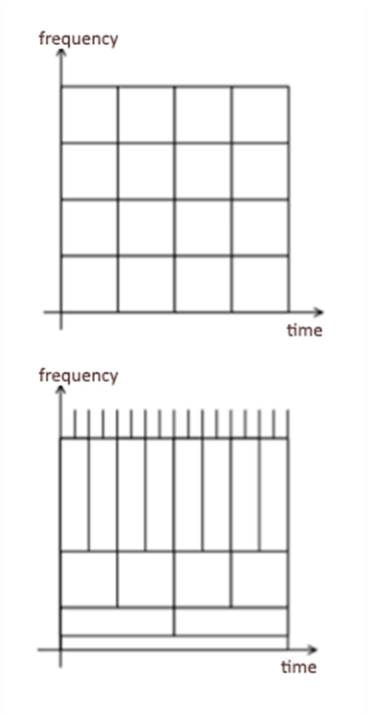

Figure 6
Frequency-time resolution of STFT and WT

6 Wavelet-Transform Profilomtery

The base of this method is to use Wavelet-transformation to determine the phase of the band-pattern. It is possible to use one-dimensional and two-dimensional transformation, however experience shows that the former one gives more accurate and faster results. In this case, one row of pixels is being analysed and repeated for each line. Since the generated patterns can be constructed from adequate modification of sinusoidal signals, the following equation can be used

$$f(x,y) = a(x,y) + b(x,y)\cos\big(2\pi f_0 x + \varphi(x,y)\big) \tag{11}$$

where $a(x,y)$ is the backlight, $b(x,y)$ is the bands amplitude, f_0 is the spatial carriers frequency, $\varphi(x,y)$ is the phase modulation of the bands. The obtaining of the depth values requires the phase and modulus, which can be calculated from the complex results of the one-dimensional continuous wavelet transformation on the examined signal:

$$\varphi(a,\tau) = tan^{-1}\left(\frac{Im(W(a,\tau))}{Re(W(a,\tau))}\right) \tag{12}$$

$$abs(a,\tau) = |W(a,\tau)| \tag{13}$$

where $Im(W(a,\tau))$ is the imaginary part, $Re(W(a,\tau))$ is the real part. The optimal values of each pixel are calculated with a direct maximum method [11], because in case of high signal-noise proportion it gives very accurate results.

The calculated phase has values in a limited range, as the inverse of trigonometric functions they can be only in the $[-\pi,+\pi)$ interval. The greater values than 2π cause artificial discontinuities, that is why we need a phase extractor, so called phase unwrap method [12]. The most common way is to examine the neighbouring pixels and regarding if the difference exceeds a given value then it add or subtract multiple of 2π, so the relative phase distance between the two pixels will be in the $[-\pi,+\pi]$ interval. The proper choice of the limits is very important, so we can filter out the noise components of the carrier and determine the three-dimensional shape of the object.

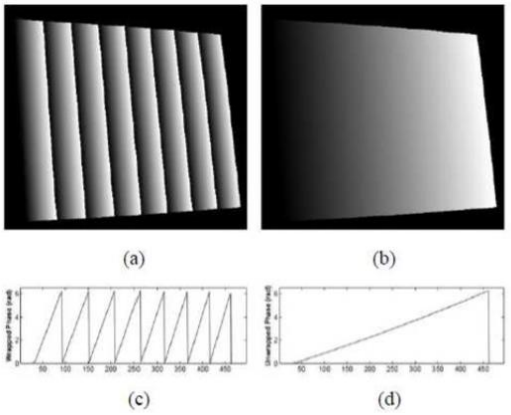

Figure 7
a) and c) Wrapped phase; b) and d) Unwrapped phase

The three-dimensional surface reconstruction is now achievable and it is performable in two different ways. With absolute coordinates we determine the position of the pixels with triangulation, which gives accurate results if we know the precise geometric parameters of the camera and the projector. The adequate calibration is time-consuming. Therefore, we can use relative coordinates, when we determine the depth values of the pixels $h(x,y)$ compared to a reference plane. The projected signal can be calculated as

$$\Delta\Phi(x) = \Phi(x) - 2\pi f_0 x, \tag{14}$$

which we can further modify to get $h(x,y)$ as well [13]:

$$\Delta\Phi(x,y) = -\frac{2\pi f_0 h(x,y) d}{l_0 - h(x,y)} \quad (15)$$

If we take the presumption that the distance between the camera and the projector is negligibly small, compared to their distance from the surface,$(l_0 \gg d)$ then we can calculate the depth information easily [14]:

$$h(x,y) = -\frac{\Delta\Phi(x,y) l_0}{2\pi f_0 d} \quad (16)$$

7 Test Frameworks with Lens

The previous experiments showed, the algorithm is working well on digitally created surfaces, but to measure its accuracy we needed a real object with measurable values. For this we chose a lens, painted it white and measured its radius with a three-ball spherometer. The painting was necessary even though it can affect the results because the method works only on non-reflecting surfaces. We used a digital projector to illuminate the object with structured sinusoidal light, which frequency was controlled by software. The image was captured with a Canon 350D DS126071 (No.1130601174) digital camera with Canon Zoom Lens EF-S 18-55.

The captured image was processed with MATLAB, because it has corresponding built-in complex Wavelet-transformations and one of the highest speeds in mathematical calculations.

7.1 Image Processing

One of the main sources of the inaccuracy is the high noise-signal ratio that is why we have to ensure that the picture is ready for arithmetical progressions by using filters and black-white-transformation. Thereafter. we choose a mother wavelet and the level of the Wavelet-transformation; transform each row of the picture; use a maximum ridge search and unwrap the phase. The depth values can be obtained by extracting a reference plane from the generated surface. It is possible to use a physical plane and process it in the same way, but this can cause more noise, so we decided to create an artificial one because in this case we have strict control over the parameters. The main properties of the pixels are the frequency and the position, so we needed to declare that:

1. The frequency of the projected pattern is known
2. The center of the loupe must be in the center of the cut picture.

As you can see in Sec. 6 we need to use a $\frac{l_0}{2\pi f_0 d}$ multiplier on the generated surface to get the depth values and set the *X* and *Y* direction multiplier for the artificial

one, so the parallel edges of the reconstructed surface will have the same values. For the evaluation we cut the middle line and searched its radius.

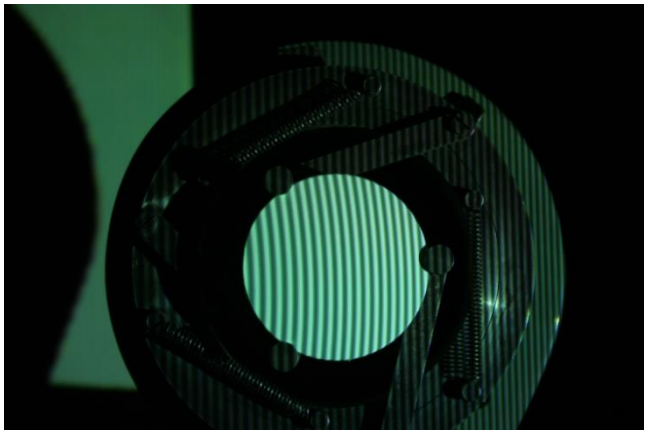

Figure 8
Captured image

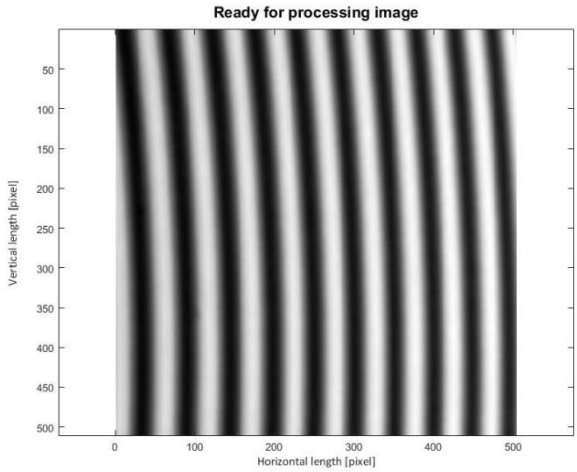

Figure 9
Ready for process image

7.2 Results

The three-ball spherometer measurement gave 390,418 mm for the radius of the lens. If the manufacturing errors were neglected we can assume that the lens has the same radius in every direction, because of its symmetry. We used the following mother wavelets with different tuning parameters: Complex Morlet,

Complex Frequency B-spline, Complex Shannon and Complex Gaussian. After the reconstruction of the surface we measured the vertical (R_y) and the horizontal (R_x) radius. The results can be seen in Table 1-4.

7.2.1 Complex Morlet Wavelets

When the tuning parameters (f_b, f_c) are set to equally 1 respectively, this method gives the best results, but it is only accurate in the vertical (R_x) direction.

Table 1
Radius of X and Y directions with Complex Morlet wavelets

	$f_b - f_c$			
CMOR	***1-0.1***	***1-0.5***	***1-1***	***1-1.5***
R_x [mm]	402.5	421.3	386.6	106.9
R_y [mm]	9.7	100	206.4	46.7

7.2.2 Complex Frequency B-spline Wavelets

The lowest error was 1,2% with 385,7 mm radius in vertical (R_x) direction. The parameters were set in this case to $f_b = 2, m = 1, f_c = 1$. The results were acceptable only in vertical direction, similar to the Morlet wavelets.

Table 2
Radius of X and Y directions with Complex Frequency B-spline wavelets

	$f_b - m - f_c$						
FBSP	***1-1-0.5***	***1-1-1***	***1-1-1.5***	***2-1-0.1***	***2-1-0.5***	***2-1-1***	***2-1-1.5***
R_x [mm]	673.1	375.4	153.5	44125.3	302.7	385.7	107.4
R_y [mm]	19.7	231.4	25.7	103.7	219.9	223.8	39.9

7.2.3 Complex Shannon Wavelets

The complex Shannon wavelets produced the highest error in the radius in both directions. The only assessable result was 3,14% error with 375,4 mm radius in the case of $f_b = 1, f_c = 1$.

Table 3
Radius of X and Y directions with Complex Shannon wavelets

	$f_b - f_c$				
SHAN	***1-0.1***	***1-0.5***	***1-1***	***1-1.5***	***2-3***
R_x [mm]	450.4	673.2	375.4	153.3	64.2
R_y [mm]	53.2	19.7	231.4	25.7	12.3

7.2.4 Complex Gaussian Wavelets

The Complex Gaussian algorithm provided the best results both in vertical (R_x) and horizontal (R_y) direction. However, the latter ones error was still intolerably high. The equation contains only one settable parameter, which gives the order of the Gauss-transformation. If we set $p=3$ (a third ordered Gauss-transformation) we can get the most accurate results, with 0,28% error with 393,0 mm radius.

Table 4

Radius of X and Y directions with Complex Gaussian Wavelets

	p							
CGAU	***1***	***2***	***3***	***4***	***5***	***6***	***7***	***8***
R_x [mm]	353.1	277.8	393	339.9	378.4	346.6	376.8	346.5
R_y [mm]	204.5	209.6	215.3	222.5	227.8	229.9	225.2	217

7.2.5 Evaluation

The projected pattern carries its waves through the transformation. Therefore. the waviness and disturbance of the reconstructed surface are making the operation less accurate. We can apply different kind of filters to eliminate this error, but they are so small that a filtering can cause relevant information loss as well.

From our goals of view we can say that the reconstruction of the object were successful, we were able to recover the radius value of the lens with small error. The Fig. 9 shows on of the best matched reconstructed surface and its middle segment which from we calculated the radius. To show the mentioned waviness we enlarged the values.

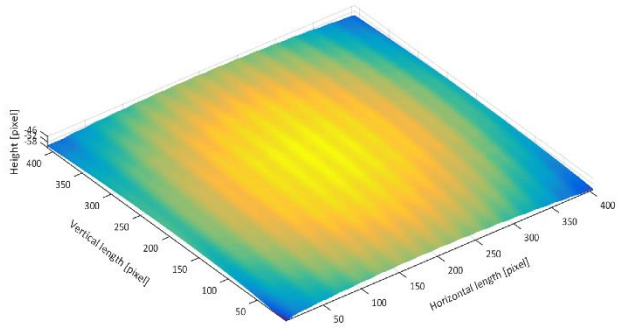

Figure 10

Enlarged reconstruction of the object with third-ordered Complex Gaussian wavelet

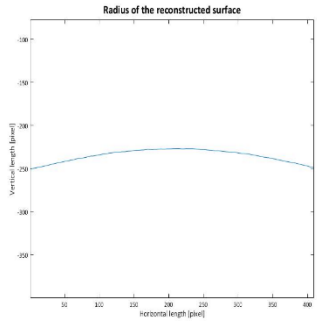

Figure 11
Middle segment to measure the radius (enlarged)

For industrial usage the method is still too slow, but the accuracy is high enough for quality control applications. That is why we choose the field of biomechatronics to create a three-dimensional reconstruction of a human back to detect spine-abnormalities.

8 Test Framework with Mannequin

A real human's back can contain many types of physical disorders, like outgrowths and birthmarks, which can cause discontinuity on the surface. Therefore, we need a "perfect" subject to widen the range of parameters and find the suitable ones. The method is following the same path: project the structured light, capture the image, cut and filter the relevant part and use Wavelet-transform analysis, but in this case with wider range of tuning parameters. The waving that can be seen in Fig. 9 is less dominant in some case, so our goal was to find an algorithm with which we can avoid this waving while keeping a level of high accuracy. We used the $\{f_b | 0.5 \leq f_b \leq 3, f_b = 0.5k, k \in \mathbb{Z}\}$ and $\{f_c | 0.5 \leq f_c \leq 3, f_c = 0.5k, k \in \mathbb{Z}\}$ intervals for the tuning parameters in the case of Complex Morlet, Complex Shannon and Complex Frequency B-spline wavelets, for the latter we used $\{0.5 \leq m \leq 2 : 0.5 \mid m\}$, and the Complex Gaussian transformation remained the same. To obtain the best reconstruction of the highest frequency needed by the projection because in this case the number of lines is the highest too and tested 152 different mother wavelets.

8.1 Evaluation

In the first step we picked the ones without errors which could have been seen with naked eyes, then cut a horizontal segment and multiplied the values, so we could have seen if they containedany waving in their minima or maxima. We then

can take this measurement as an ideal back reconstruction and choose 8 mother wavelets which can be used for later usage:

- Complex Morlet($f_b = 0{,}5;\ f_c = 1{,}5$)
- Complex Morlet($f_b = 1;\ f_c = 1$)
- Complex Morlet($f_b = 1{,}5;\ f_c = 1$)
- Complex Morlet($f_b = 2;\ f_c = 1$)
- Complex Frequency B-spline ($f_b = 2; m = 0{,}5;\ f_c = 0{,}5$)
- Complex Frequency B-spline ($f_b = 2; m = 1{,}5;\ f_c = 1$)
- Complex Frequency B-spline ($f_b = 2; m = 1;\ f_c = 1$)
- Complex Gaussian ($p = 8$)

Fig. 11 and Fig. 12 shows that the reconstruction can be implemented with good approximation, but this is measured by shaping the function and selected with naked human eyes, so we need more experiments with measurable test subjects. To do this we used a real human body with spine-disorder, called scoliosis, and calculated the correlation between the digitally reconstructed spine shape and a radiogram.

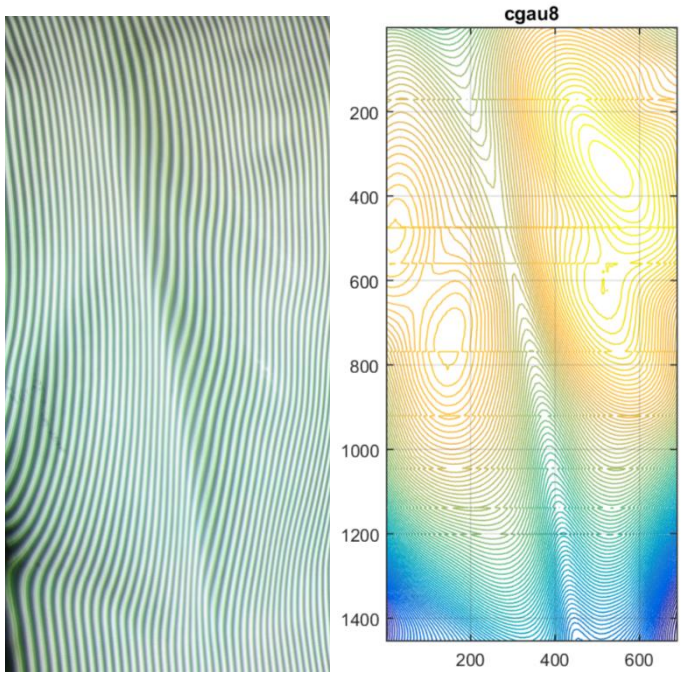

Figure 12
Reconstructed mannequin back with 8th order Complex Gaussian Wavelet

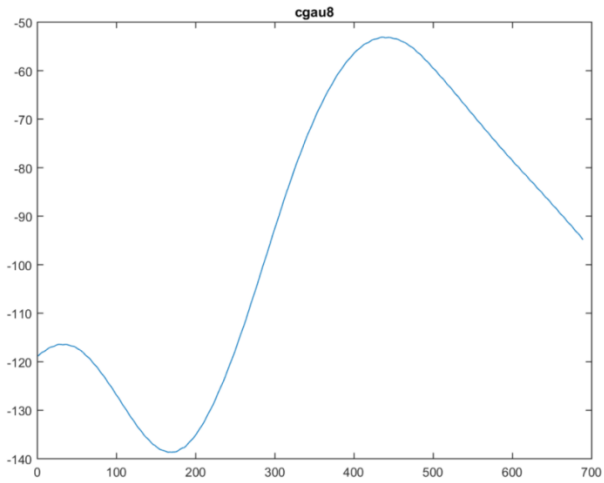

Figure 13
Horizontal segment of the reconstructed surface without equal axis

9 Test Framework with Living Subject

9.1 Spine Deformation Types

The human spine contains 33 small bones called vertebrae, and their connection creates a natural curve, which runs straight down from the back and located in the middle of the back. It can absorb the stress from external impacts like movements and weight, therefore, its deformation has huge physiological effect [15]. We can distinguish three main type of the deformations:

- **Scoliosis**: The spine has a sideway curve so it becomes S- or C-shaped (Fig. 13a).
- **Kyphosis**: The back is abnormally rounded, the curvature has more than 50 degrees in it (Fig. 13b)
- **Lordosis**: Also called as swayback, because it has a significant inward curving of the spine at the lower back (Fig. 13c)

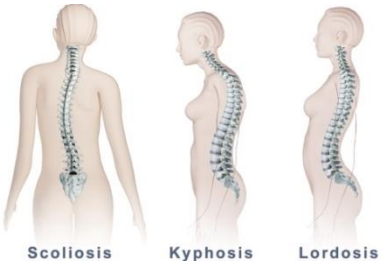

Figure 14
Types of spine deformations: a) Scoliosis, b) Kyphosis, c) Lordosis [16]

9.2 Examination of the Spine Shape from WTP

The procedure was the same as before: project the pattern, capture the image, cut and filter, then reconstruct the surface – in this case her back - with Wavelet-transform profilometry. Our subject was a 24 year old girl with slight scoliosis. To measure the accuracy we needed to determine the spine curving and fit a polynomial on it.

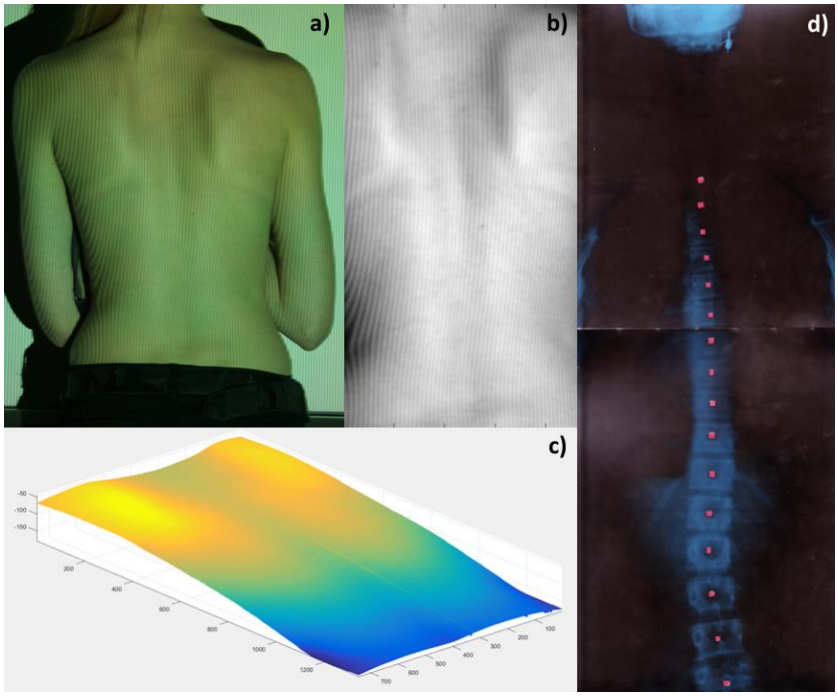

Figure 15
a) Tested back with slight scoliosis, b) Ready to process image, c) Reconstructed surface with 8th order Complex Gaussian Wavelet, d) Radiogram from the spine

As it can be seen in Fig. 13a the scoliosis causes a sideway curve so it forms a S- or C-shape that is why we approximated this curve with a cubic polynomial. We tried to find the deepest point of each line of the reconstructed surface and fit a polynomial on the points. We had an assumption that the deepest point of the row must be in a certain interval, if not then it would break the spine continuity. Therefore, that point cannot be on the spine.

9.3 Examination of the Spine Shape from Radiogram

To calculate the inaccuracy we needed an etalon, which was a radiogram from the subject's back. Although the radiogram was taken 6 years ago, our subject did not participate in any kind of treatment, so her back did not change a lot since then. After considering this information, we set a goal to reach of less than 30% difference between the x-dependent coefficients.

The scanned radiogram (Fig. 14d) is not clear enough to detect the vertebra easily with image processing techniques. So, we decided to use markers on it by sticking red dots on the middle of the vertebra and read their coordinates. For better results we did not use all the markers to fit polynomial on, only the ones which are part of the S-shape.

9.4 Evaluation of the Results

Some of the polynomials were far-out of the acceptable limits, it could be seen even with naked eyes. The Complex Morlet Wavelet gave the lowest difference between the coefficients, 26,64% with $f_b = 1{,}5, f_c = 1$ and 29,47% with $f_b = 2$ $f_c = 1$. In the case of 8th order Complex Gaussian Wavelet the differences were 50,8%, which is not suitable anymore.

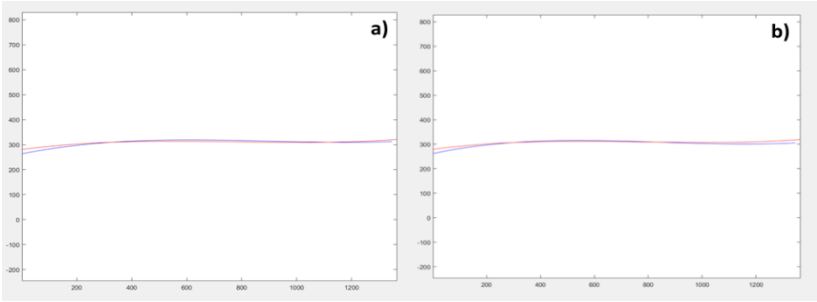

Figure 16
Reconstructed spine shape with a) CMOR (1,5-1) and b) CMOR (2-1) blue: polynomial from WTP; red: polynomial from the radiogram

10 Development Opportunities

First of all we would like to terminate the waving hereby reach higher accuracy in the horizontal direction. There are some methods for this, but all of them reduce the vertical direction accuracy. The other development opportunity is to use a higher resolution camera to capture the image, but the higher amount of pixel results higher processing time as well. Further development opportunity is to use machine learning algorithm to set the variables of this method with an advanced controller [17] to create embedded systems.

Conclusions

In this paper we presented the well-known Fringe Projection Technique solutions. We also did some measurements, where this technique was tested on a lens, and a human body. In the first case the best solution was chosen from the used Wavelets, we got the closest result using Complex Gaussian Wavelets. The best solution happened with the third ordered Gauss transformation. The measured radius of the examined lens was 390.42 mm, using this CGAU Wavelet we got a very close 393.00 mm result.

On a real human we also tried this profilometric technique, the used Wavelets were the Complex Morlet (with 4 different settings), the Complex Frequency B-Spline (with 3 different settings), and the Complex Gaussian (p=8). The best solution originated from the Complex Morlet Wavelet, where $f_b = 1{,}5, f_c = 1$. The Complex Gaussian gave us a huge inaccuracy. It can be stated that in this case the Complex Gaussian Wavelet is not the right choice.

In this work we successfully applied the Wavelet-transform profilometry in surface identification. By lower noise-signal ratio the Complex Gaussian wavelet provided the best results, but as we enlarged this ratio by scanning a real human back the Complex Morlet Wavelet had higher accuracy. As the research shows the WTP can be adapted well for the current environment by using different mother wavelets, so it could be applied in many other industrial fields as well.

Acknowledgement

This work was supported by Budapest University of Technology and Economics, Department of Mechatronics, Optics and Mechanical Engineering Informatics. K. Péter acknowledges the support of Nikolett Kerékgyártó for being the subject by the biomechatronical tests and give free run of using her radiogram.

References

[1] M. Takeda, H. Ina, and S. Kobayashi, “Fourier-Transform Method of Fringe-Pattern Analysis for Computer-Based Topography and Interferometry,” J Opt Soc Am, Vol. 72, No. 1, pp. 156-160, 1982

[2] M. Takeda, K. Mutoh, and S. Kobayashi, “Fourier-Transform Profilometry for the Automatic-Measurement of 3-D Object Shapes,” Appl Optics, Vol. 22, No. 24, pp. 3977-3982, 1983

[3] D. J. Bone, H. A. Bachor, and R. J. Sandeman, "Fringe-Pattern Analysis Using a 2-D Fourier-Transform," Appl Optics, Vol. 25, No. 10, pp. 1653-1660, 1986

[4] P. Balla, P. Kocsis, Gy. Eigner, Á. Antal, "Surface reconstruction with Wavelet transformation", 20th Jubilee International Conference on Intelligent Engineering Systems, Jun 20-July 2, 2016, Budapest

[5] Dr. Ábrahám György: Optika, 1998, Panem Kft. kiadó

[6] Yong Xu, Shuhai Jia, Qingchen Bao, Hualing Chen and Jia Yang, "Recovery of absolute height from wrapped phase maps for fringe projection profilometry", Optics express, 2014

[7] S. G. Mallat, "A theory for multiresolution signal decomposition: The wavelet representation," University of Pennsylvania, Tech. Rep., 1987

[8] A. Z. Abid, M. A. Gdeisat, D. R. Burton, and M. J. Lalor, "Ridge extractionalgorithms for one-dimensional continuous wavelet transform: acomparison," Journal of Physics - Conference Series, Vol. 76, No. 1, pp.1-7, 2007

[9] Y. Meyer, Wavelets, Algorithms & Applications, 1st ed. Philadelphiam, USA: SIAM, 1993

[10] P. Hariharan, Basics of Interferometry, 2nd ed. San Diego, USA: Academic Press, 2007

[11] A. Z. Abid, M. A. Gdeisat, D. R. Burton, and M. J. Lalor. (2016) A comparison between wavelet fringe analysis algorithms. [Online]. Available: photon06archive.iopconfs.org/FASIG%203%20Wed%2016.30.doc

[12] A. Rene, W.L.H. Carmona, and T. Brun, "Characterization of Signals by the Ridges of Their Wavelet Transforms," IEEE T Signal Proces, Vol. 45, No. 10, pp. 2586-2590, 1997

[13] R. Talebi, J. Johnson, and A. Abdel-Daye, "Binary code pattern unwrapping technique on fringe projection method," in Proceedings of the 17th International Conference on Image Processing, Computer Vision, & Pattern Recognition (IPCV'13), p. P7

[14] Z. Zhang and J. Zhong, "Applicability analysis of wavelet- transform profilometry," Opt Express, Vol. 21, pp. 18 777-18 796, 2013

[15] P. Balla, G. Manhertz, Á. Antal, "Diagnostic moiré image evaluation in spinal deformities", Optica Applicata, Vol. XLVI, No. 3, pp. 375-385, 2016

[16] https://therapeutixmassage.com/detection-treatment-spine-deformity-scoliosis/ (20178.01.18)

[17] Gy. Eigner, "Control of Physiological Systems Through Linear Parameter Varying Framework", Acta Polytechnica Hungarica, Vol. 14, No. 6, 2017, pp. 185-212